**Rosenfeldt, S, Stoter, M, Schlenk, M, Martin, T, Queiroz De Albuquerque, R, Foster, S and Breu, J**

**In Depth Insights into the Key Steps of Delamination of Charged 2D Nano Materials**

# In Depth Insights into the Key Steps of Delamination of Charged 2D Nano Materials

***Sabine Rosenfeldt,[1] Matthias Stöter[2], Mathias Schlenk[1], Thomas Martin[2], Rodrigo Queiroz Albuquerque,[3] Stephan Förster,*[1] and Josef Breu*[2]***

[1] Physical Chemistry I, University of Bayreuth, Universitätsstrasse 30, 95440 Bayreuth, Germany

[2] Inorganic Chemistry I, University of Bayreuth, Universitätsstrasse 30, 95440 Bayreuth, Germany

[3] São Carlos Institute of Chemistry, University of São Paulo, Av. Trab. Sao-carlense 400, 13560-970 São Carlos, Brazil.

**ABSTRACT:**

Delamination is a key step to obtain individual layers from inorganic layered materials needed for fundamental studies and applications. For layered van-der-Waals materials like graphene the adhesion forces are small allowing for mechanical exfoliation, whereas for ionic layered materials like layered silicates the energy to separate adjacent layers is considerably higher. Quite counter intuitively, we show for a synthetic layered silicate ($Na_{0.5}$-hectorite) that a scalable and quantitative delamination by simple hydration is possible for high and homogeneous charge density, even for aspect ratios as large as 20000. A general requirement is the separation of adjacent layers by solvation to a distance where layer interactions become repulsive (Gouy-Chapman length). Further hydration up to 34 nm leads to the formation of a highly ordered lamellar liquid crystalline phase (Wigner crystal). Up to 8 higher-order reflections indicate excellent positional order of individual layers. The Wigner crystal melts when the interlayer separation reaches the Debye length, where electrostatic interactions between adjacent layers are screened. The layers become weakly charge-correlated. This is indicated by fulfilling the classical Hansen-Verlet and Lindeman criteria for melting. We provide insight into the requirements for layer separation and controlling the layer distances for a broad range of materials and outline an important pathway for the integration of layers into devices for advanced applications.

**KEYWORDS:** delamination, monolayer formation, nanosheet, small-angle X-ray scattering, hectorite

## Introduction

Two-dimensional (2D) materials have an atomic organization where the bond strengths along two dimensions are much stronger compared to the third dimension (1). The crystal structures typically consist of thin layers of atoms with strong directional bonding within the layers and much weaker interactions between the layers. If the layers are neutral, they form van-der-Waals solids with only weak layer interaction. Prominent examples for these materials are graphene and transition metal dichalcogenides such as $MoS_2$, $WS_2$ or $WSe_2$. For charged layers such as in layered silicates the layer interactions are much stronger. Exfoliated or delaminated nanosheets of 2D-materials have unusual phononic (2), electronic (3, 4), ferroic (5), electrochemical (6), and mechanical properties (7, 8) which are used in phononics, photovoltaics, semiconductors and electrodes. Those properties are strongly tied to the limitation or annihilation of translational symmetry along the stacking direction. When individual monolayers are homogeneously dispersed in a matrix, the related composite materials have a maximized, huge surface-to-volume ratio, and for large aspect ratios (ratio of diameter to layer thickness) these materials process a very small percolation threshold to provide electrical and thermal conductivity, mechanical strength, and large tortuous paths for diffusion barriers. Therefore, control over the layer thickness and interlayer distance is essential. For van-der-Waals solids the weak interlayer interaction energies (4 – 7 kJ/mol) can be overcome by mechanical forces (mechanical exfoliation). A simple and prominent case being the exfoliation of graphene layers using “Scotch tape” (9). The “Scotch tape” method is, however, limited to fundamental research in small scale. Various other techniques ranging from epitaxial growth to mechanical exfoliation, potentially assisted by surface active compounds or by rendering the starting material more shear labile by intercalation reactions, have been shown to yield 2D materials. Established techniques, however, tend to produce broad distributions of layers (5, 10-12) because separation by mechanical exfoliation is incomplete and, moreover, usually comes along with breakage of the layers.

The same conclusions are valid for the exfoliation of ionic layers, where the exfoliation process is even more difficult due to the stronger attractive interactions between the layers, which are of the order of 100 kJ/mol and larger. Separation procedures almost exclusively rely on mechanical exfoliation with the aid of intercalation of large ions, molecules or surface active compounds, albeit with generally poor and incomplete exfoliation. Even in case of high shear rates, the aspect ratio is never reaching its intrinsic maximum defined by the pristine lateral extension of the inorganic stacks. Alternatively, osmotic swelling potentially represents a gentler, cheap and scalable route to utterly separate a layered material into singular layers.

The principle of osmotic swelling goes back to the swelling of graphite oxide (1932) (13) and montmorillonite (14). Here we report a systematic study of the exfoliation of a synthetic 2D layered silicate via osmotic swelling that provides direct insight into the conditions for ionic layer separation and the build-up of the electric double layer, and outlines the lyotropic phase behavior at extreme aspect ratios of the resulting layered material over more than 4 orders of magnitude in concentration from the dry powder to highly dilute solutions.

**Results and Discussions**

Osmotic delamination is known empirically to require a well-defined homoionic layered material with high and very homogeneous charge density. Natural layered silicates suffer from pronounced charge density modulations at all length scales (15). Even synthetic layered silicates when synthesized at temperatures below 1000 K show a non-uniform intracrystalline reactivity. As a consequence, a large fraction of the stacks does not show osmotic swelling at all, or the separation between adjacent layers varies randomly and a weighted average of the *d*-spacings is observed which is of limited analytical and practical value (16). Moreover, all the above mentioned materials need to be ion-exchanged and/or purified in some way prior to osmotic swelling. For instance, for montmorillonite a selective dissolution of amorphous auxiliary minerals like iron oxihydroxids is applied, where concomitantly ion exchange occurs and homoionic Na-montmorillonite is obtained (17). Following purification, the ionic strength needs to be reduced and finally the suspensions need to be re-concentrated physically, e.g. by sedimentation or centrifugation, to solid contents where liquid crystalline (LC) phases are observed. For kinetic reasons during the concentration procedure equilibrium structures might not be readily achieved (18).

Here we use a synthetic hectorite with a composition in the unit cell of $[Na_{0.96}]^{inter}[Mg_{5.14}Li_{0.94}]^{oct}[Si_8]O_{20}F_4$ (two formula units per unit cell and therefore abbreviated as $Na_{0.5}$-hectorite) that has been synthesized from the melt at temperatures well above 1000 K (19). The material does not require any purification and shows a very homogeneous intracrystalline reactivity. With this material at hand, delamination and swelling can be studied starting with a 1D crystalline dry powder all the way into the LC regime and beyond simply by adding increasing amounts of water.

**Regime I: Crystalline Swelling (attractive)**

The first steps of layer separation occur via discrete hydration steps as indicated by the adsorption isotherm (Fig. 1a) of synthetic $Na_{0.5}$-hectorite (19). The transitions from non-hydrated (0-WL) to the first water layer (1-WL) and the second water layer (2-WL) occur at threshold partial pressures of $p/p_0 = 0.22$ and $p/p_0 = 0.64$, respectively. The observed hysteresis indicates that the phase transitions are first-order, which is also suggested by MD-

simulations (26-28). All structures consist of equidistant layers with long-range 1D ordering within a stack which is referred to as a tactoid. Adjacent layers are stacked in an uncorrelated mode (turbostratic stacking). For more highly charged layered silicates in some rare cases three-dimensionally ordered phases can be obtained making crystal structure solutions of 1-WL and 2-WL hydrates available (20, 21).

In the 1-WL state an inner sphere Na-hydrate complex is observed where $Na^+$ is in direct contact with basal oxygen atoms on one side, due to Coulomb attraction, and is coordinated by three water molecules on the other side. In the 2-WL state an outer sphere hexaaquo-$Na^+$-complex occupies the middle of the interlayer space with symmetrical hydrogen bonding to both adjacent basal oxygen planes (20).

For the more highly charged synthetic hectorite, the 3-WL structure is not accessible within the experimentally accessible humidity range. It has been observed for natural montmorillonites of lower charge density, i.e. $\sigma_s = 0.66$ charges per $nm^2$, where the hexaaquo-$Na^+$-complexes were found to predominantly stay in close contact with only one of the silicate layer surfaces (22). To verify this configuration for the synthetic $Na^+$-hectorite, we performed MD-simulations of the 3-WL structure. Details of the calculations are given in the Supporting Information. We found that 30% of the $Na^+$-cations were coordinated to the basal oxygens and formed an inner-sphere complex, similar as in the 1-WL structure. 64% formed hexaaquo-$Na^+$-cations located at distances of 0.24 Å away from the surface, similar as in the 2-WL structure. Additionally, 6% formed a hexaaquo-$Na^+$-complex in the center of the interlayer space. Upon increasing hydration (0-WL → 1-WL → 2-WL → 3-WL) we observe a structural evolution from surface associated non-hydrated via partially and fully hydrated counterions to finally surface detached counterions. In the 3-WL phase the surface separated counterions start localizing in the midplane between the two surfaces. This represents the build-up of the classical counterion double layer structure (Grahame model) with a sequence of three layers: (a) The first layer is the inner Helmholtz plane, where the counter ions are located at the charged surface, (b) followed by an outer Helmholtz plane with surface-separated, fully hydrated ions, and (c) a diffusive double layer with non-localized ions at the midplane (where the electric field vanishes). A full development of the diffuse double layer would eventually lead to electrostatic repulsion, (22, 23) driving the separation of adjacent layers.

**Transition I: Crystalline to Osmotic Swelling**

To obtain insight into the conditions for separation of charged layers, as a first approximation the relevant interaction energies and length scales are estimated from simple physical models:

a) For ion-ion interactions the important length scale is the Bijerrum length

$$l_B = \frac{e^2}{4\pi\varepsilon\varepsilon_0 k_B T} \quad (1)$$

which is the distance at which Coulomb interactions between ions are equal to the thermal energy $k_B T$. $e$ is the elementary charge, $\varepsilon_0$ the vacuum permittivity, and $\varepsilon$ the dielectric constant. Taking water ($\varepsilon = 78$) at $T = 298.15$ K (25°C), the Bijerrum length is equal to $l_B = 0.71$ nm.

b) For ion-surface interactions the relevant length scale is the Gouy-Chapman length

$$l_{GC} = \frac{1}{2\pi l_B \sigma_s} \quad (2)$$

the distance of an ion to a charged surface where electrostatic surface-ion interactions are equal to the thermal energy. $\sigma_s$ is the surface charge density (in units of 1/m$^2$). For a charge density of 1 charge per nm$^2$ (0.96 charges per 2($a$×$b$) = 0.95 nm), as in the present system, the Gouy-Chapman length is equal $l_{GC} = 0.22$ nm.

c) As a measure of the degree of electrostatic coupling of the ions to the surface, one defines a coupling parameter (24)

$$\Xi = \frac{l_B}{l_{GC}} \quad (3)$$

where in case of $\Xi >> 1$ the counterions are strongly coupled to the surface. For the present case we have $\Xi = 3.2$ such that the surface-coupling of counterions is significant.

d) The Debye length for the case of monovalent ions is given by

$$\kappa^{-1} = \left( \frac{\varepsilon\varepsilon_0 k_B T}{2 N_A e^2 c_I} \right)^{1/2} \quad (4)$$

and is the length scale beyond which electrostatic interactions are screened. If no specific measures are taken to remove ionic impurities from aqueous solutions, one has a typical ion concentration of $c_I = 10^{-4}$ mol/l which corresponds to a Debye length of $\kappa^{-1} = 30$ nm.

These electrostatic length scales will be related to the layer surface separation $h$ to distinguish different regimes with characteristic properties.

The onset of repulsion of adjacent silicate layers is related to the trade-off between short-range attractive electrostatic interactions, hydration forces, and counterion translational entropy. For small $h$ in the order of the Gouy-Chapman length ($h \approx l_{GC}$,Regime I) we have a competition between attractive surface-counterion interactions with an energy $F_{el} \approx -hk_BT / l_{GC}$ and a repulsive entropic contribution due to the translational entropy of the counterions, given by $F_S \approx k_BT \ln h$, which is increasing with increasing layer surface separation $h$. Both contributions result in an osmotic pressure between the surfaces given by (24)

$$\Pi = \sigma_s \frac{\partial F}{\partial d} \approx l_{GC}\sigma_s k_B T\left(\frac{2l_{GC}}{h} - 1\right) \quad (5)$$

For layer surface separation $h > 2l_{GC} = 0.44$ nm according to this simple model, repulsive interactions are expected.

For layered silicates, the initial separation during crystalline swelling is driven by the strong hydration forces, which for $Na^+$ involve an energy of 406 kJ/mol. With the silicate layer thickness of 0.96 nm as determined by the interlayer distance of non-hydrated $Na_{0.5}$-hectorite (19), the 2-WL structure would already be expected to be in the repulsive regime ($h \approx 1.55 - 0.96nm = 0.59nm > 2l_{GC}$). Experimentally, 2-WL is found to be still stabilized at a discrete hydration state. Yet, the value of 0.59 nm is not significantly larger than the estimated threshold of 0.44 nm, as secondary attractive interactions such as lateral or specific ion or solvent correlations, van der Waals interactions and hydrogen bonding were neglected. For the 3-WL structure, $h \approx 1.83 - 0.96nm = 0.87nm$, the repulsive regime is finally entered. The interactions applied in the MD simulation are more realistic and correctly indicated the transition to the repulsive regime with the 3-WL structure. The calculations predict that layer charge variations or inhomogeneities, which directly affect $l_{GC}$, may easily lead to a situation where domains with repulsive and attractive interactions coexist within a layer. Even when there is a small fraction of the latter, it will prevent the separation of adjacent layers by osmotic swelling. This problem becomes increasingly severe with increasing lateral diameter of the tactoids relevant for practical applications.

**Regime II: Osmotic Swelling in the Gouy-Chapman Regime**

After the attractive short-range surface-ion interactions have been overcome by hydration such that $h >> 2l_{GC}$, repulsive interactions between the layers dominate. Further addition of water will then lead to a continuous further separation of the layers. This regime is

characterized by the length scales $l_D >> h >> l_{GC}$. This regime is referred to as **Gouy-Chapman regime**. Here the osmotic pressure between adjacent layers separated by a distance *h* is given by (24)

$$\Pi \approx \frac{\pi k_B T}{2 l_B} \frac{1}{h^2} \qquad (6)$$

and thus becomes independent of the surface charge density $\sigma_s$ and the related ion-surface interactions. The osmotic pressure is now dominated by ion-ion interactions characterized by the Bijerrum length $l_B$ and is quite long-ranged, i.e. proportional to $h^{-2}$.

As suggested by this model, with addition of water the layers completely separate and the silicate/water mixture forms transparent gels. Gel formation has been noticed as early as in the 1930s and at that time was related to the “house-of-cards” model, a connected network of edge-basal plane interactions of layers (23). An alternative interpretation of the gel phase has been proposed by Langmuir in 1938 who described it as a lamellar lyotropic phase (25). This has been later confirmed by Michot and Miyamoto (2006) for a series of layered silicates including nontronite, montmorillointe (26-28), beidellite (29), laponite (18), fluorotetrasilicic mica (30) and fluorohectorite (30, 31). Lamellar lyotropic phases were also found by *Gabriel et al*. in 2001 for a solid acid, $H_3Sb_3P_2O_{14}$ (32), and by *Geng et. al.* for $H_{0.8}[Ti_{1.2}Fe_{0.8}]O_4 \bullet H_2O$ (33).

The pristine sample in the dried state represents a statistically isotropic microcrystalline sample with mean tactoid diameters of 18 µm and heights of typically 1.5 µm (Fig. S1). The uniquely homogeneous charge density and intracrystalline reactivity of the synthetic $Na_{0.5}$-hectorite, now allowed a systematic investigation of osmotic swelling by small-angle X-ray scattering (SAXS, Fig. 2 a,b and Figs. S3). Consistent with the observation of Langmuir, Michot and Miyamoto, 2D-scattering patterns of the bulk samples show a series of concentric, equidistant diffraction rings which are characteristic for lamellar lyotropic structures. The scattering patterns are highly anisotropic due to shear-alignment of the highly swollen tactoids during filling of the gels in the X-ray capillary. A high scattering intensity is found at the equator indicating that the layers align parallel to the surface of the vertically mounted capillary. A quantitative analysis applying model calculations reveal orientational order parameters as high as $S = 0.8$ (see table S1, Supporting Information).

In Fig. 2b the azimuthally averaged data are given. For higher concentrations we observe a rational series (1:2:3:…) of *00l*-reflections indicating the formation of a lyotropic lamellar phase. Up to 8 higher order reflections underline the excellent positional order of adjacent individual layers. Upon dilution the peak positions shift to lower *q*-values, indicating

increasing separation of the silicate layers due to progressing swelling. The interlayer distance reaches values up to 170 nm for ϕ = 0.002. The observed $q^{-2}$-scaling of the scattering intensity over nearly the whole scattering curve confirms the presence of thin layers with very large lateral dimensions. For the higher concentrations, where the signal-to-noise ratio is higher, it is possible to determine the first minimum of the form factor oscillations at high *q* (Fig. 2b), which allows to derive the thickness of the layers to $d_0 = 0.85$ nm. This is slightly smaller than the monolayer thickness of 0.96 nm obtained from the interlayer distance of non-hydrated $Na_{0.5}$-hectorite (19), because small-angle X-ray scattering is sensitive to the high homogeneous electron density of the silicate core layer.

The solid lines are quantitative fits to the measured scattering intensities using a model of stacked layers where the scattered intensity is given by (39)

$$I(q) = b^2 \rho P(q, d_0, D_0)\left[1 + \beta(q)\left(Z(q, d, D) - 1\right)G(q, \delta)\right] \quad (7)$$

where $b$ is the scattering contrast between the silicate layers and the solution, $\rho$ the number density of the layers, *q* the scattering vector, $P(q)$ the form factor, $d_0$ the layer thickness and $D_0$ the lateral layer dimension. $Z(q)$ is the lattice factor determining the interlayer distance (or lamellar long period) $d$ as well as the peak width, which is related to the lateral size $D$ of the ordered domains. $G(q)$ is the Debye-Waller factor, which depends on the mean deviation $\delta$ of the layers from their ideal lattice point. The term $S(q) = \left[1 + \beta(q)\left(Z(q, d, D) - 1\right)G(q, \delta)\right]$ is the structure factor, which will be discussed in a separate section. The measured scattering intensities could be well fitted to this expression to determine the layer thickness $d_0 = 0.85$ nm and the lamellae spacing, while keeping the lateral layer dimension $D_0 = 18$ μm, which was determined by electron microscopy, constant. The data are summarized in Table S1 in the Supporting Information.

The λ-shaped *11/02*-band (asterisk in Fig. 2b) is observed for all dilutions at the same q-values (q ~ 1.4 $Å^{-1}$), indicating that the (*hk*)-plane structure of the silicate layers are not influenced by the swelling in the *00l* direction of the tactoids. The lamellar distance is plotted as a function of volume fraction in Fig. 2d. For high volume fractions $\phi > 0.025$ we observe a linear dependence following $d = d_0 / \phi$ typical for lamellar systems (25) corroborating monolayers uniformly separated by water. As a result of strong repulsive interactions the layers localize on a highly ordered lattice, thereby maximizing their separation. This homogeneous single gel phase of highly swollen tactoids phenomenologically resembles a Wigner crystal, which is observed for electrons in plasmas, when their repulsive interactions

become much larger than their kinetic energy such that they couple, become positionally strongly correlated and localize on lattice points with the maximum possible inter-electron distance.

**Transition II: Melting of Wigner Crystal (Delamination)**

The scaling relation given in Fig. 2d shows a kink at $\phi = 0.025$. Below this volume fraction a weaker concentration dependence of the layer distance, $d \sim \phi^{-0.66}$, is observed indicating the transition to a more disordered regime. At the same concentration any induced shear orientation observed in 2D SAXS pattern relaxes upon cessation of shear (Fig. S3). Further, the relative lattice derivations from the lattice points $\delta$ reaches values over 10% (cf. table S1). According to the Lindeman-criterium (34) lattice melting is expected for relative displacements larger than 10%. In good agreement with all the other criteria the structure factor (Fig. 2c) confirms the melting transition, fulfilling the Hansen-Verlet criterion according to which the melting transition corresponds to a value of $S(q) = 2.85$. Larger values correspond to ordered solid, smaller values to a molten solid. This value is crossed at a volume fraction of $\phi = 0.025$. This shows that for $d \sim \kappa^{-1}$, the Wigner lattice melts due to the screening of the long-range electrostatic interaction.

**Regime III: Osmotic Swelling in the Screened Regime**

When the interlayer distance becomes larger than the Debye-length $\kappa^{-1} \approx 30$ nm, a new regime characterized by $h >> \kappa^{-1}, l_{GC}$ is reached. Here, electrostatic interactions are screened beyond length scales of $l_D$ and the osmotic pressure is given by

$$\Pi \approx \frac{8 k_B T \kappa^2}{\pi l_B} e^{-d/l_D} \tag{8}$$

with a strongly screened repulsive interaction. (24) The weakening of electrostatic repulsion at transition II leads to reduced correlations of adjacent layers and melting of the Wigner crystal. As a consequence, in regime III a weaker concentration dependence of the interlayer distance, namely $d \sim \phi^{-0.66}$ (Fig. 2d) is observed. For lyotropic liquid-crystalline phases of conventional molecular surfactants or block-copolymers, a change in the exponential of the equation $d \sim \phi^{-\beta}$ signals a transition between different topologies: $\beta = 1$, $\beta = 1/2$, and $\beta = 1/3$ for lamellar, cylindrical (rod like), and spherical topologies, respectively. An isotropic phase with freely rotating layers would be signalled by $\beta = 1/3$. A value of $\beta = 2/3$ would be characteristic of a bicontinuous phase (35, 36).

As such topological changes cannot occur for insoluble silicate layers, at this point the physical reason behind the $\beta = 0.66$ dependency is unclear. *Michot et al.* observed for size classified nontronite also a discontinuity of the scaling from $\phi^{-1}$ to a variety of different slopes, depending on the size fraction (27). The observed slopes were therefore described by a mixture of freely rotating small platelets scaling with $\phi^{-1/3}$ and a lyotropic lamellar phase of larger platelets scaling with $\phi^{-1}$. Although $Na_{0.5}$-hectorite is also polydisperse, the smallest diameters seen in static laser scattering are still in the micron range (19). Hence the $\phi^{-1/3}$ can only be observed for $d > 1$ μm and freely rotating layers therefore can be ruled out at $d$-spacings where the discontinuity ($d^* \approx 34$ nm) is observed.

The change in the exponent indicates phase separation. Yet, macroscopically we do not observe phase separation in regime III at concentrations $0.025 < \phi < 0.0015$. Rather, the gels seem to undergo microphase segregation, where an ordered lamellar microphase of silicate layers (phase A) is in equilibrium with a disordered microphase of higher water content (phase B), which leads to a weaker concentration dependence of the layer distance $d$. In phase B separated, but not freely rotating layers are expected to have a folded and undulated conformation reducing the effective lateral extension, thereby gaining conformational entropy which drives the phase separation.

Individual layers can separate from a lamellar stack or tactoid via an unbinding transition. This is known for amphiphilic lamellar systems, where lamellae unbind and detach from the top of a lamellar stack and then separate. They then fold, similar to the silicate layers, but then subsequently close to form vesicles, such that there is a concentrated ordered lamellar phase in equilibrium with a dilute vesicular phase.

Alternatively, individual layers within the lamellar stack or tactoid could translate laterally beyond the former crystal edges of the tactoid and then fold and gain conformational entropy, thereby increasing its effective diameter. The tactoid would then remain intact upon dilution, which we observe by polarized optical video microscopy (see Supporting Information). While expanding the interlayer space, the morphology of the tactoid is gradually converted from a platelet to a wormlike rod. The pristine tactoids typically have an aspect ratio of 12 (Fig. S4). The aspect ratio is then inverted to 0.2 at a separation of the individual silicate layers of about 60 nm ($\phi \approx 0.01$). At these late stages of osmotic swelling the electrostatic repulsion between adjacent layers is increasingly screened, such that the electro-steric repulsion between adjacent tactoids becomes significant, also because with the inversion of the aspect ratio, the relative contribution of tactoid edge surface to basal surface interaction increases drastically.

Regime III is characterized by increasing widths and decreasing intensities of the Bragg peaks, indicating a reduction of the coherence length in the ordered domains, and loss of higher order reflections, corresponding to larger deviations from the lattice points. For very dilute solutions eventually the peaks would be at very low q-values, out of the range of our SAXS-setup, with a $q_{min}$ corresponding to d ~ 170 nm and $\phi > 0.0023$.

At $\phi = 0.0015$, the suspension is still viscous with no macroscopic phase separation as indicated by polarized light imaging. Experimentally, we observed no visible phase separation even over periods of several months. It may nevertheless be that at much longer periods (> 1 year) and despite very slow kinetics segregation might occur (37). Below this volume fraction the two microphases start to macroscopically phase separate by gravitation as shown in Fig. 3 and Fig. S5. Interestingly, for suspensions with $0.0008 < \phi < 0.0004$ (Fig. 3b-d) after two days phase separation results in a layered superstructure with textures with periodicities of several millimeters. At further dilution tactoids with smaller lateral diameters will eventually start to rotate freely and be present in the supernatant phase, whose volume increases with progressing dilution (Fig. 3b-f).

Eventually, upon sufficient dilution a single dilute phase will be reached if the layer separation is of the order of the lateral dimension of the layers, e.g. if $\phi \sim \frac{d_0}{D_0}$. Due to the high median aspect ratio of 18000, this concentration is calculated to be extremely small, i.e. $\phi \sim 0.000056$. Indeed, a suspension close to this concentration ($\phi = 0.00009$) appears to be a single phase. It is shear-birefringent because there is still shear-induced alignment of the layers (Fig. S6) , but the birefringence disappears after cessation of shear.

**Conclusions:**

In conclusion we show that the delamination of charged layers requires that the layer separation exceeds the Gouy-Chapman length ($h > 2l_{GC}$) such that interactions between adjacent layers become repulsive, leading to an osmotic swelling. In the electrostatically attractive regime ($h \sim l_{GC}$) layer separation occurs by discrete hydration steps. During initial steps of osmotic swelling the classical double layer structure consisting of an inner and outer Helmholtz plane followed by a diffuse double layer is established. Upon further hydration there is a regime of strong osmotic-repulsion (Gouy-Chapman regime), where the layers form a highly ordered one-dimensional Wigner crystal. When the interlayer distances reaches the Debye-length, a new regime with screened osmotic repulsion is entered, accompanied by a melting of the Wigner crystal and formation of a first microscopically

phase separated system. Macroscopic phase separation by gravitation does not set in until much lower concentrations ($\phi < 0.0015$). At very low concentrations ($\Phi$<~0.0001) finally a homogeneous dilute phase is reached.

Our study reveals the conditions for charged layer exfoliation, provides insight into why high charge density and charge homogeneity are crucial, how the electric double layers is established, and describes the structure and property of the resulting lamellar in the limit of extreme aspect ratios, which is relevant for applications e.g. as fillers in nanocomposite films used as gas barrier.

**Acknowledgments**

The financial support from the German Research Foundation, in the frame of the Collaborative Research Center (SFB 840): “From particulate nanosystems to mesotechnology” is highly acknowledged.

**Referencess**

1. Blackmore, A. V.; Miller, R. Tactoid size and osmotic swelling in calcium montmorillonite. *Soil Sci. Soc. Amer. Proc.* **1961**, 25, 169-173.

2. Chiritescu, C.; Cahill, D. G.; Nguyen, N.; Johnson, D.; Bodapati, A.; Keblinski, P.; Zschack, P. Ultralow thermal conductivity in disordered, layered WSe2 crystals. *Science* **2007**, 315, 351-353.

3. Takada, K.; Sakurai, H.; Takayama-Muromachi, E.; Izumi, F.; Dilanian, R. A.; Sasaki, T. Superconductivity in two-dimensional CoO2 layers. *Nature* **2003**, 422, 53-55.

4. Novoselov, K. S.; Geim, A. K.; Morozov, S. V.; Jiang, D.; Zhang, Y.; Dubonos, S. V.; Grigorieva, I. V.; Firsov, A. A. Electric field effect in atomically thin carbon films. *Science* **2004**, 306, 666-669.

5. Wu, W.; Wang, L.; Li, Y.; Zhang, F.; Lin, L.; Niu, S.; Chenet, D.; Zhang, X.; Hao, Y.; Heinz, T. F.; Hone, J.; Wang, Z. L. Piezoelectricity of single-atomic-layer MoS2 for energy conversion and piezotronics. *Nature* **2014**, 514, 470-474.

6. Mashtalir, O.; Naguib, M.; Mochalin, V. N.; Dall'Agnese, Y.; Heon, M.; Barsoum, M. W.; Gogotsi, Y Intercalation and delamination of layered carbides and carbonitrides. *Nat Commun* **2013**, 4, 1716.

7. Suk, J. W.; Piner, R. D.; An. J.; Ruoff, R. S. Mechanical Properties of Mono layer Graphene Oxide. *Acs Nano* **2010**, 4, 6557-6564.

8. Kunz, D. A.; Feicht, P.; Goedrich, S.; Thurn, H.; Papastavrou, G.; Fery, A.; Breu, J. Space-Resolved In-Plane Moduli of Graphene Oxide and Chemically Derived Graphene Applying a Simple Wrinkling Procedure. *Adv Mater* **2013**, 25, 1337-1341.

9. Novoselov, K. S.; Jiang, D.; Schedin, F.; Booth, T. J.; Khotkevich, V. V.; Morozov, S. V.; Geim, A. K. Two-dimensional atomic crystals. *Proc Natl Acad Sci USA* **2005**, 102, 10451-10453.

10. Butz, B.; Dolle, C.; Niekiel, F.; Weber, K.; Waldmann, D.; Weber, H. B.; Meyer, B.; Spiecker, E. Dislocations in bilayer graphene. *Nature* **2014**, 505, 533-537.

11. Kim, S. S.; Van Khai, T.; Kulish, V.; Kim, Y. H.; Na, H. G.; Katoch, A.; Osada, M.; Wu, P.; Kim, H. W. Tunable Bandgap Narrowing Induced by Controlled Molecular Thickness in 2D Mica Nanosheets. *Chem Mater* **2015**, 27, 4222-4228.

12. Lotya, M.; Hernandez, Y.; King, P. J.; Smith, R. J.; Nicolosi, V.; Karlsson, L. S.; Blighe, F. M.; De, S.; Wang, Z. M.; McGovern, I. T.; Duesberg, G. S.; Coleman, J. N. Liquid Phase Production of Graphene by Exfoliation of Graphite in Surfactant/Water Solutions. *J Am Chem Soc* **2009**, 131, 3611-3620.

13. Hofmann, U. Eindimensionale Quellung von Graphitsäure und Graphit. Die Reaktionsweisen des Graphits. *Kolloid Z* **1932**, 61, 297-304.

14. Hofmann, U.; Kurd, E.; Diederich, W. Kristallstruktur und Quellung von Montmorillonit (Das Tonmineral der Bentonittone). *Z Kristallogr* **1933**, 86, 340-348.

15. Lagaly, G. Characterization of Clays by Organic-Compounds. *Clay Miner* **1981**, 16, 1-21.

16. Ferrage, E.; Lanson, B.; Sakharov, B. A.; Geoffroy, N.; Jacquot, E.; Drits, V. A. Investigation of dioctahedral smectite hydration properties by modeling of X-ray diffraction profiles: Influence of layer charge and charge location. *Amer Mineral* **2007**, 92, 1731-1743.

17. Mehra, O. P.; Jackson, M. L. Iron oxide removal from soils and clays by dithionite-citrate system buffered with sodium bicarbonate. *Clays Clay Miner* **1958**, 7, 317-327.

18. Paineau, E.; Bihannic, I.; Baravian, C.; Philippe, A. M.; Davidson, P.; Levitz, P.; Funari, S. S.; Rochas, C.; Michot, L. J. Aqueous Suspensions of Natural Swelling Clay Minerals. 1. Structure and Electrostatic Interactions. *Langmuir* **2011**, 27, 5562-5573.

19. Stöter, M.; Kunz, D. A.; Schmidt, M.; Hirsemann, D.; Kalo, H.; Putz, B.; Senker, J.; Breu, J. Nanoplatelets of Sodium Hectorite Showing Aspect Ratios of ~ 20000 and Superior Purity. *Langmuir* **2013**, 29, 1280-1285.

20. Kalo, H.; Milius, W.; Breu, J Single Crystal Structure Refinement of One- and Two-layer Hydrate of Sodium-Fluorohectorite. *RSC Adv* **2012**, 2, 8452-8459.

21. Kalo, H.; Milius, W.; Bräu, M.; Breu, J. Synthesis and single crystal structure refinement of the one-layer hydrate of sodium brittle mica. *J. Solid State Chem.* **2013**, 198, 57-64.

22. Skipper, N. T.; Lock, P. A.; Titiloye, J. O.; Swenson, J.; Mirza, Z. A.; Howells, W. S.; Fernandez-Alonso, F. The structure and dynamics of 2-dimensional fluids in swelling clays. *Chem Geo.* **2006**, 230, 182-196.

23. Hofmann, U.; Hausdorf, A. Kristallstruktur und innerkristalline Quellung des Montmorillonits. *Z Kristallogr* **1942**, 104, 265-293.

24. Naji, A.; Jungblut, S.; Moreira, A. G.; Netz, R. R Electrostatic interactions in strongly-coupled soft matter. *Physica A* **2005**, 352, 131-170.

25. Langmuir, I. The Role of Attractive and Repulsive Forces in the Formation of Tactoids, Thixotropic Gels, Protein Crystals and Coacervates. *J Chem Phys* **1938**, 6, 873-896.

26. Michot, L. J.; Bihannic, I.; Maddi, S.; Funari, S. S.; Baravian, C.; Levitz, P.; Davidson, P. Liquid-crystalline aqueous clay suspensions. *Proc Natl Acad Sci USA* **2006**, 103, 16101-16104.

27. Michot, L. J.; Bihannic, I.; Maddi, S.; Baravian, C.; Levitz, P.; Davidson, P. Sol/gel and isotropic/nematic transitions in aqueous suspensions of natural nontronite clay. Influence of particle anisotropy. 1. Features of the I/N transition. *Langmuir* **2008**, 24, 3127-3139.

28. Michot, L. J.; Baravian, C.; Bihannic, I.; Maddi, S.; Moyne, C.; Duval, J. F. L.; Levitz, P.; Davidson, P. Sol-Gel and Isotropic/Nematic Transitions in Aqueous Suspensions of Natural Nontronite Clay. Influence of Particle Anisotropy. 2. Gel Structure and Mechanical Properties. *Langmuir* **2009**, 25, 127-139.

29. Paineau, E.; Antonova, K.; Baravian, C.; Bihannic, I.; Davidson, P.; Dozov, I.; Imperor-Clerc, M.; Levitz, P.; Madsen, A.; Meneau, F.; Michot, L. J. Liquid-Crystalline Nematic Phase in Aqueous Suspensions of a Disk-Shaped Natural Beidellite Clay. *J Phys Chem B* **2009**, 113, 15858-15869.

30. Miyamoto, N.; Iijima, H.; Ohkubo, H.; Yamauchi, Y. Liquid crystal phases in the aqueous colloids of size-controlled fluorinated layered clay mineral nanosheets. *Chem Commun* **2010**, 46, 4166-4168.

31. Hemmen, H.; Ringdal, N. I.; De Azevedo, E. N.; Engelsberg, M.; Hansen, E. L.; Meheust, Y.; Fossum, J. O.; Knudsen, K. D. The Isotropic-Nematic Interface in Suspensions of Na-Fluorohectorite Synthetic Clay. *Langmuir* **2009**, 25, 12507-12515.

32. Gabriel, J. C.; Camerel, F.; Lemaire, B. J.; Desvaux, H.; Davidson, P.; Batail, P. Swollen liquid-crystalline lamellar phase based on extended solid-like sheets. *Nature* **2001**, 413, 504-508.

33. Geng, F.; Ma, R.; Nakamura, A.; Akatsuka, K.; Ebina, Y.; Yamauchi, Y.; Miyamoto, N.; Tateyama, Y.; Sasaki, T. Unusually stable ~100-fold reversible and instantaneous swelling of inorganic layered materials. *Nat Commun* **2013**, 4:1632.

34. Lindemann, F. A. The calculation of molecular vibration frequencies. *Z Phys* **1910**, 11, 609-615.

35. Hyde, S. T. in *Handbook of Applied Surface and Colloid Chemistry*, ed. Holmberg, K. (John Wiley & Sons, Chichester), **2001**, pp. 299-332.

36. Hyde, S. T. Swelling and structure. Analysis of the topology and geometry of lamellar and sponge lyotropic mesophases. *Langmuir* **1997**, 13, 842-851.

37. Ruzicka, B.; Zaccarelli, E.; Zulian, L.; Angelini, R.; Sztucki, M.; Moussaid, A.; Narayanan, T.; Sciortino, F. Observation of empty liquids and equilibrium gels in a colloidal clay. *Nat Mater* **2011**, 10, 56-60.

38. Breu, J.; Seidl, W.; Stoll, A. J.; Lange, K. G.; Probst, T. U. Charge homogeneity in synthetic fluorohectorite. *Chem Mater* **2001**, 13, 4213-4220.

39. Förster, S.; Fischer, S.; Zielske, K.; Schellbach, C.; Sztucki, M.; Lindner, P.; Perlich, J. Calculation of scattering-patterns of ordered nano- and mesoscale materials. *Adv Colloid Interface Sci* **2011**, 163, 53-83.

40. Martinez, L.; Andrade, R.; Birgin, E.; Martinez, J. PACKMOL: A Package for Building Initial Configurations for Molecular Dynamics Simulations. *J Comput Chem* **2009**, 30, 2157-2164.

41. Plimpton, S. Fast Parallel Algorithms for Short-Range Molecular-Dynamics. *J Comput Phys* **1995**, 117, 1-19.

42. Cygan, R. T.; Liang, J. J.; Kalinichev, A. G. Molecular models of hydroxide, oxyhydroxide, and clay phases and the development of a general force field. *J Phys Chem B* **2004**, 108, 1255-1266.

43. Marry, V.; Dubois, E.; Malikova, N.; Durand-Vidal, S.; Longeville, S.; Breu, J. Water Dynamics in Hectorite Clays: Infuence of Temperature Studied by Coupling Neutron Spin Echo and Molecular Dynamics. *Environ Sci Technol* **2011**, 45, 2850-2855.

44. Berendsen, H. J. C.; Grigera, J. R.; Straatsma, T. P. The Missing Term in Effective Pair Potentials. *J Phys Chem* **1987**, 91, 6269-6271.

45. Humphrey, W.; Dalke, A.; Schulten, K. VMD: Visual molecular dynamics. *J Mol Graph* **1996**, 14, 33-38.

**Figure Legends**

**Figure 1.** (a) Water vapor sorption isotherm of $Na_{0.5}$-hectorite and corresponding hydrated structures of 0-, 1-, 2-WL hydrates. (b) histogram of the Z-distribution of $Na^+$ (black bars) and oxygens ("$O_w$", yellow bars) of water molecules in the interlayer space of the hectorite obtained during 1 ns of MD simulation (NVT, 300 K). Red bars represent the plane of basal oxygens of the tetrahedral layers. The five blue gaussians are the deconvoluted peaks of the black bars.

**Figure 2:** (a) 2D-SAXS pattern at volume fraction $\phi$ = 0.059. On the right side, experimental data are plotted, on the left side modelled patterns are shown. (b) The one-dimensional (1D) SAXS intensity show a shift of the *001* reflection to higher *d*-spacings with decreasing concentration and the concentration independent position of the *hk*-band (asterisk) at high q. (a. $\phi$ = 0.090 (red pentagons); b: $\phi$ = 0.035 (blue hexagons); c: $\phi$ = 0.024 (magenta crosses),

d: $\phi = 0.010$ (green squares) and e: $\phi = 0.0016$ (black triangles). Calculated scattering curves and the $q^{-2}$-scaling law of layers are given by solid lines. (c) Structure factor of swollen lyotropic phases at different volume fractions. a) $\phi = 0.003$; b) $\phi = 0.007$; c) $\phi = 0.010$, d) $\phi = 0.017$, e) $\phi = 0.024$, f) $\phi = 0.030$; g) $\phi = 0.035$; h) $\phi = 0.059$; I) $\phi = 0.090$. The dashed line at S(q) = 2.85 marks the Hansen-Verlet rule where melting is expected. (d) Scaling relation *d*-spacing as a function of volume fraction. The solid line corresponds to a 1D-swelling law following the equation $d = D/\phi$, which fits both crystalline swelling and Wigner crystal regime. The gradient in the nematic sol regime (dashed line) follows a distinct scaling ($d \sim \phi^{-0.66}$).

**Fig. 3:** Macroscopic phase separation of $Na_{0.5}$-hectorite suspensions observed between crossed polarizer and analyzer. (a) $\phi = 0.0015$; (b) $\phi = 0.0008$; (c) $\phi = 0.0005$; (d) $\phi = 0.0004$; (e) $\phi = 0.0003$; (f) $\phi = 0.0002$.

**Figure 1:**

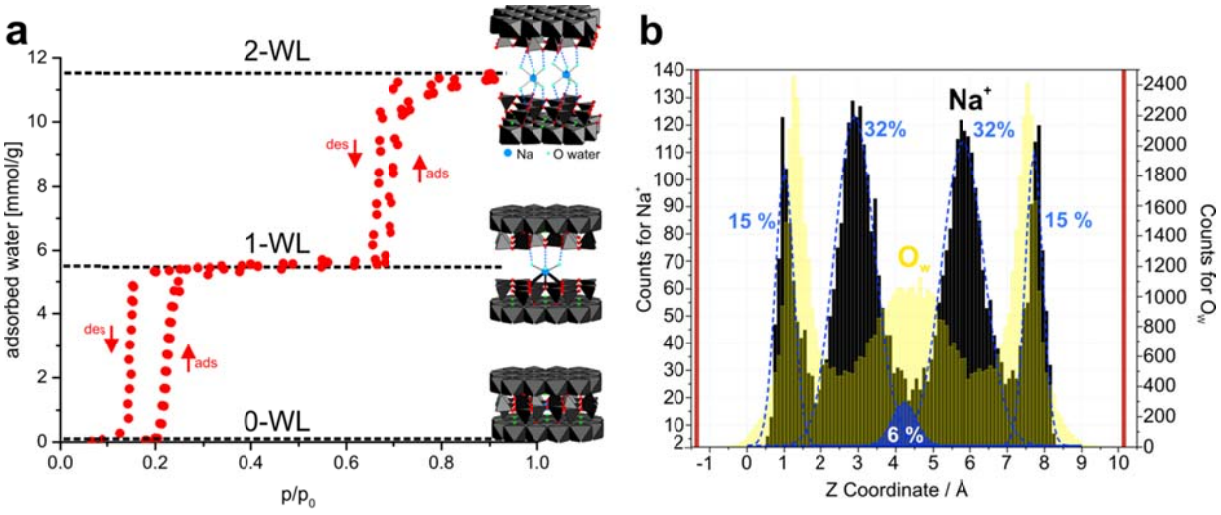


**Figure 2:**

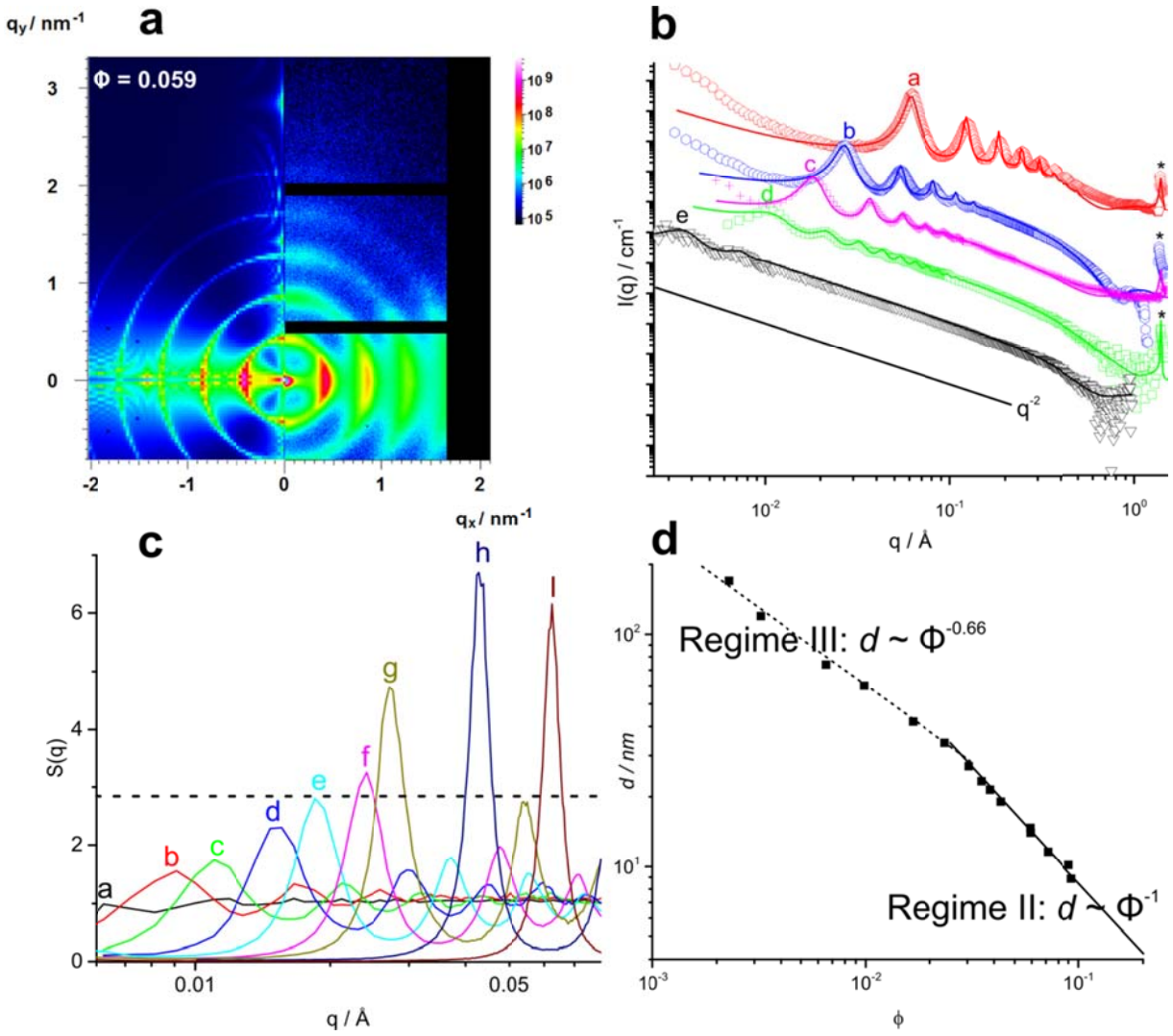

**Figure 3:**